Atmospheric
Chemistry
and Physics
Discussions

1   # A Possible Pathway for Rapid Growth of Sulfate during Haze Days in China

2
3   Guohui Li[1*], Naifang Bei[2], Junji Cao[1*], Rujin Huang[1*], Jiarui Wu[1], Tian Feng[1,2], Yichen Wang[1], Suixin Liu[1],
4   Qiang Zhang[3], Xuexi Tie[1], and Luisa T. Molina[4]
5
6   [1]Key Lab of Aerosol Chemistry and Physics, SKLLQG, Institute of Earth Environment, Chinese Academy of
7   Sciences, Xi'an, China
8   [2]School of Human Settlements and Civil Engineering, Xi'an Jiaotong University, Xi'an, Shaanxi, China
9   [3]Department of Environmental Sciences and Engineering, Tsinghua University, Beijing, China
10 [4]Molina Center for Energy and the Environment, La Jolla, CA, and Massachusetts Institute of Technology,
11   Cambridge, MA, USA
12 [*]Correspondence to: Guohui Li (ligh@ieecas.cn), Junji Cao (jjcao@ieecas.cn), and Rujin Huang
13 (Rujin.Huang@psi.ch)
14
15

16 **Abstract**: Rapid industrialization and urbanization have caused frequent occurrence of haze

17 in China during wintertime in recent years. The sulfate aerosol is one of the most important

18 components of fine particles ($PM_{2.5}$) in the atmosphere, contributing significantly to the haze

19 formation. However, the heterogeneous formation mechanism of sulfate remains poorly

20 characterized. Observed filter measurements of $PM_{2.5}$, sulfate, and iron, and relative humidity

21 in Xi'an, China have been employed to evaluate the mechanism and to develop a

22 parameterization of the sulfate heterogeneous formation involving aerosol water for

23 incorporation into atmospheric chemical transport models. Model simulations with the

24 proposed parameterization can successfully reproduce the observed sulfate rapid growth and

25 diurnal variations in Xi'an and Beijing, China. Reasonable representation of sulfate

26 heterogeneous formation in chemical transport models considerably improves the $PM_{2.5}$

27 simulations, providing the underlying basis for better understanding the haze formation and

28 supporting the design and implementation of emission control strategies.

29

30

31

32

Atmospheric
Chemistry
and Physics
Discussions

1   Introduction

33

34   Sulfate is a main component of aerosols or fine particles ($PM_{2.5}$) in the atmosphere and

35   plays a key role in global climate change. The direct and indirect radiative effects induced by

36   sulfate aerosols have constituted one of the major uncertainties in current assessments of

37   climate change (IPCC, 2013). In addition, deposition of sulfate aerosols exerts deleterious

38   impacts on ecosystems through acidification of soils, lakes, and marshes (e.g., Schindler,

39   1988; Gerhardsson et al., 1994). Sulfate is also an important contributor to the haze formation

40   and substantially reduces the atmospheric visibility during hazy days (e.g., He et al., 2014;

41   Guo et al., 2014).

42   The main source of sulfate in the atmosphere is the oxidation of sulfur dioxide (SO_2)，

43   which is directly emitted from fossil fuel combustion, industrial processes, and volcanoes, or

44   generated by oxidation of other sulfur-containing species, such as dimethyl sulfide (DMS).

45   The conversion of SO_2 to sulfate involves various processes, including gas-phase oxidations

46   by hydroxyl radicals (OH) and stabilized criegee intermediates (sCI) (Mauldin III et al.,

47   2012), aqueous reactions in cloud or fog droplets, and heterogeneous reactions associated

48   with aerosols (Seinfeld and Pandis, 2006).

49   Model studies have been performed to investigate the formation of sulfate aerosols on

50   global or regional scales (Barrie et al., 2001). Previous global model results, considering the

51   contribution of SO_2 gas-phase oxidation and aqueous reactions in cloud or fog droplets driven

52   by ozone (O_3) and hydrogen peroxide (H_2O_2), have suggested that SO_2 mixing ratios are

53   generally overestimated while sulfate concentrations tend to be underestimated, indicating

54   that the two SO_2 oxidation pathways still cannot close the gap between field observations and

55   modeling studies (Kasibhatla et al., 1997; Laskin et al., 2003). Incorporation of aqueous SO_2

56   oxidation by oxygen catalyzed by transition metal ions in models has improved sulfate

57   simulations compared to measurements (Jacob and Hoffmann, 1983; Jacob et al., 1984, 1989;

Atmospheric
Chemistry
and Physics
Discussions

58   Pandis and Seinfeld, 1992; Alexander et al., 2009), and recent studies have further shown the

59   enhanced role of transition metal ions catalysis during in-cloud oxidation of SO_2 (Harris et al.,

60   2013). However, models still underestimate SO_2 oxidation in winter source regions due to

61   lack of cloud or fog or a missing oxidation mechanism (Feichter et al., 1996; Kasibhatla et al.,

62   1997; Barrie et al., 2001). Therefore, heterogeneous conversion of SO_2 to sulfate associated

63   with aerosols provides a possible pathway for improving the sulfate simulations in chemical

64   transport models (CTMs) (Kasibhatla et al., 1997; Zhang et al., 2015).

65   Many experimental studies have been conducted to investigate the heterogeneous

66   reactions of SO_2 on various model oxides and mineral dust, but the underlying sulfate

67   formation mechanism is still not comprehensively understood. Generally, the complicated

68   sulfate heterogeneous formation from SO_2 is parameterized as a first-order irreversible uptake

69   by aerosols in CTMs, with a reactive uptake coefficient ranging from 10^{-4} to 0.1 and also

70   heavily depending on relative humidity in the atmosphere (Wang et al., 2014). It is still

71   imperative to develop a ubiquitous parameterization of the SO_2 heterogeneous reaction to

72   reasonably represent sulfate formation in CTMs.

73   In recent years, China has experienced frequently severe and persistent haze pollutions

74   caused by elevated $PM_{2.5}$ concentrations, and field measurements have shown that sulfate

75   aerosols are one of the most important species in $PM_{2.5}$ (He et al., 2014; Tian et al., 2016).

76   Reasonable representation of sulfate aerosols provides underlying basis for $PM_{2.5}$ simulations.

77   Laboratory experiments, field measurements, and model simulations have significantly

78   advanced our understanding of SO_2 heterogeneous reactions in the atmosphere, providing a

79   good opportunity to develop a parameterization to more reasonably represent the sulfate

80   formation in CTMs. In this study, a parameterization for sulfate formation from SO_2

81   heterogeneous reactions has been developed based on the daily filter measurements in Xi'an

82   since 2003, and verified using the Weather Research and Forecast model with Chemistry

83   (WRF-CHEM) in Xi'an and Beijing, China.

84

85   **2   Model and Methodology**

86   **2.1   WRF-CHEM Model**

87   In the present study, a specific version of the WRF-CHEM model (Grell et al., 2005) is

88   utilized to assess the proposed heterogeneous sulfate parameterization, which is developed by

89   Li et al. (2010, 2011a, b, 2012) at the Molina Center for Energy and the Environment. A new

90   flexible gas phase chemical module is incorporated into the model to consider different

91   chemical mechanisms, and the CMAQ/Models3 aerosol module developed by US EPA is

92   adopted for aerosol simulations. Chemical species surface dry depositions are parameterized

93   following Wesely (1989), and the wet deposition is calculated using the method in the

94   CMAQ. The photolysis rates are calculated using the FTUV in which the aerosol and cloud

95   effects on photolysis are included (Li et al., 2005; Li et al., 2011a).

96   The ISORROPIA Version 1.7 (Nenes et al., 1998) is used to predict inorganic aerosols

97   in the WRF-CHEM model. A non-traditional SOA module is employed to calculate

98   secondary organic aerosol (SOA) formation, including the volatility basis-set (VBS)

99   modeling method in which primary organic components are assumed to be semi-volatile and

100   photochemically reactive and are distributed in logarithmically spaced volatility bins. The

101   SOA contributions from glyoxal and methylglyoxal are also considered as a first-order

102   irreversible uptake by aerosol particles and cloud droplets in the model. Detailed information

103   can be found in Li et al. (2011b).

104   Two persistent heavy haze pollution episodes are selected in the present study: (1)

105   December 16 to 27, 2013 in the Guanzhong basin (GZB); and (2) January 13 to 21, 2014 in

106   Beijing-Tianjin-Hebei (BTH) (Figure 1). Detailed model configurations and aerosol species

107   observation sites are given in Table 1.

108 **2.2 Statistical Methods for Comparisons**

109   The mean bias (*MB*) and the index of agreement (*IOA*) are used to evaluate the

110 performance of the WRF-CHEM model in simulating gas-phase species and aerosols against

111 measurements. The *IOA* varies from 0 to 1, with 1 indicating perfect agreement of the

112 prediction with the observation.

113    $MB = \frac{1}{N}\sum_{i=1}^{N}(P_i - O_i)$

114    $IOA = 1 - \frac{\sum_{i=1}^{N}(P_i - O_i)^2}{\sum_{i=1}^{N}(|P_i - \bar{O}| + |O_i - \bar{O}|)^2}$

115 where P_i and O_i are the calculated and observed pollutant concentrations, respectively. *N* is

116 the total number of the predictions used for comparisons, and $\bar{P}$ and $\bar{O}$ represents the average

117 of the prediction and observation, respectively.

118 **2.3 Pollutants Measurements**

119   The hourly near-surface NO_2, SO_2, and $PM_{2.5}$ mass concentrations in GZB and BTH

120 are released by the China's Ministry of Environmental Protection (China MEP) and can be

121 downloaded from the website http://www.aqistudy.cn/. The daily filter measurements of

122 aerosol species have been performed since 2003 at the Institute of Earth Environment,

123 Chinese Academy of Sciences (hereafter referred to as IEECAS, 34.23°N, 108.88°E) in Xi'an,

124 China (Figure 1a). The sulfate, nitrate, ammonium, and organic aerosols are measured by the

125 Aerodyne High Resolution Time-of-Flight Aerosol Mass Spectrometer (HR-ToF-AMS) with

126 a novel $PM_{2.5}$ lens from 13 December 2013 to 6 January 2014 at IEECAS site in Xi'an and

127 from 9 to 26 January 2014 at the Institute of Remote Sensing and Digital Earth, Chinese

128 Academy of Sciences (40.00°N, 116.38°E) in Beijing (Figure 1b). Detailed information about

129 the HR-ToF-AMS measurement can be found in Elser et al. (2016).

130

131 **3 Results and Discussions**

132 **3.1 Parameterization of SO₂ Heterogeneous Reaction Involving Aerosol Water**

Atmospheric
Chemistry
and Physics
Discussions

133   Figure 2 shows the scatter plot of the wintertime sulfate and $PM_{2.5}$ daily mass

134   concentrations at IEECAS from 2003 to 2010. The wintertime is defined as December of the

135   year to February of the next year. The observed daily $PM_{2.5}$ mass concentrations frequently

136   exceed 150 μg m^{-3} during wintertime, showing that Xi'an has experienced heavy air pollution.

137   The sulfate aerosols constitute about 15.7% of the $PM_{2.5}$ mass concentration on average, and

138   the occurrence frequency with the daily sulfate mass concentration exceeding 50 μg m^{-3} is

139   around 25.7%.

140   The observed high level of sulfate aerosols is hardly interpreted using SO_2 gas-phase

141   oxidations by OH and sCI due to the low O_3 level in the winter. The insolation is weak during

142   wintertime in North China, unfavorable for photochemical activities. The O_3 formation is

143   slow and the observed O_3 concentrations are very low, particularly during haze episodes. The

144   real-time hourly measurements of O_3 and $PM_{2.5}$ concentrations during 2013 and 2015

145   wintertime are analyzed as follows in GZB (5 cities, 39 sites, Figure 1a), which are released

146   by China MEP since 2013. Values of the hourly $PM_{2.5}$ concentrations ([$PM_{2.5}$]) are first

147   subdivided into 20 bins with the interval of 25 μg m^{-3}. O_3 concentrations ([O_3]) in the 5 cities

148   as [$PM_{2.5}$] are assembled, and an average of [O_3] in each bin are calculated (Nakajima et al.,

149   2001; Kawamoto et al., 2006). As shown in Figure 3, when [$PM_{2.5}$] increase from 10 to 75 μg

150   m^{-3}, [O_3] significantly decrease from around 41 to 23 μg m^{-3}; when [$PM_{2.5}$] exceed 200 μg m^{-}

151   ^{3}, [O_3] fluctuate between 18 and 21 μg m^{-3}. The average [O_3] in the 5 cities during the 2013

152   and 2015 wintertime are 27 μg m^{-3} (about 13.5 ppbv). Considering the determining role of O_3

153   in the formation of OH and sCI in the atmosphere, the very low level of [O_3] during

154   wintertime significantly reduces the efficiency of the sulfate formation from SO_2 oxidation

155   by OH and sCI.

156   Humid conditions have been observed to facilitate the sulfate formation in the

157   atmosphere (e.g., Sun et al., 2013; Zheng et al., 2015). Figure 4 presents the scatter plot of the

Atmospheric
Chemistry
and Physics
Discussions

Open Access

EGU

158   wintertime sulfate at IEECAS and the relative humidity (RH) at an adjacent meteorological

159   station from 2003 to 2010. The observed sulfate displays a positive correlation with the RH

160   with the correlation coefficient of 0.70, indicating that the aerosol water induced by the

161   aerosol wet growth might play an important role in the sulfate formation. It is worthy to note

162   that since high RH often coincides with stagnation, the concentrations of a lot of pollutants

163   also build up during high RH periods. There are two possible pathways for the sulfate

164   formation: bulk aqueous-phase oxidation of SO_2 in aerosol water and heterogeneous reaction

165   of SO_2 on aerosol surfaces involving aerosol water.

166   The heterogeneous reaction of SO_2 on dust surfaces has been investigated

167   comprehensively, but the sulfate formation mechanism is still not completely understood.

168   Possible mechanisms have been proposed that mineral dust and NO_2 enhance the conversion

169   of SO_2 to sulfate (He et al., 2014; Xie et al., 2015; Xue et al., 2016). Size-segregated particle

170   samples in Beijing have shown that a considerable amount of sulfate is distributed in the

171   coarse mode with particle diameters ranging from 2.1 to 9 μm, but sulfate peak

172   concentrations still occur in the fine mode with particle diameters ranging from 0.43 to 1.1

173   μm (Tian et al., 2016). Oxidation of sulfite by NO_2 in aerosol water has also been proposed to

174   contribute considerably to the sulfate production when NH_3 concentrations are sufficiently

175   high (Pandis and Seifeld, 1989; Xie et al., 2015).

176   Laboratory or field studies have suggested that O_3 or Fe^{3+} can oxidize sulfite to sulfate.

177   Considering the low [O_3] during wintertime (Figure 3), the oxidation of sulfite by O_3 cannot

178   constitute the main source of the wintertime sulfate. Mineral dust and coal combustion in

179   China could provide sufficient iron. Measurements have indicated that mineral dust accounts

180   for about 10% of $PM_{2.5}$ in Beijing (He et al., 2014). Observations at an urban site in Ji'nan,

181   China have also shown enhanced iron concentrations during haze episodes, ranging from 0.7

182   to 5.5 μg m^{-3}, which are primarily emitted from steel smelting and coal combustion (Wang et

Atmospheric
Chemistry
and Physics

Open Access

EGU

Discussions

183 al., 2012). Figure 5 shows the scatter plot of the wintertime $PM_{2.5}$ and iron at IEECAS site

184 from 2003 to 2010. The iron mass concentration generally increases with $[PM_{2.5}]$, varying

185 from 0.1 to 10 µg m^{-3}, but does not correlate well with the $[PM_{2.5}]$ with the correlation

186 coefficient of 0.34, showing considerable background contributions. We assume that 1% of

187 iron in Xi'an is dissolved in aerosol water and 1% of dissolved iron is in the Fe^{3+} oxidation

188 state (Alexander et al., 2009). When the aerosol water concentration varies from 100 to 1000

189 µg m^{-3}, the Fe^{3+} concentrations in Xi'an are between 0.18 and 180 µM, providing favorable

190 conditions for the oxidation of adsorbed sulfite (Seinfeld and Pandis, 2006).

191   We propose here a SO_2 heterogeneous reaction parameterization in which the SO_2

192 oxidation in aerosol water by O_2 catalyzed by Fe^{3+} is limited by mass transfer resistances in

193 the gas-phase and the gas-particle interface.

194      $$S(IV) + \frac{1}{2}O_2 \xrightarrow{Fe^{3+}} S(VI)$$
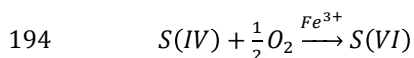
195 When the solution pH is between 5.0 and 7.0, the oxidation reaction is second order in

196 dissolved iron and first order in S(IV) and can be expressed as follows (Seinfeld and Pandis,

197 2006):

198      $$-\frac{d[S(IV)]}{dt} = 1 \times 10^{-3}[S(IV)] \quad 5.0 < pH < 6.0$$

199      $$-\frac{d[S(IV)]}{dt} = 1 \times 10^{-4}[S(IV)] \quad pH \sim 7.0$$

200 where [S(IV)] is the sulfite (S(IV)) concentration. The measured SO_2 mass accommodation

201 coefficient on aqueous surfaces is around 0.1 (Worsnop et al., 1989). Due to sufficient NH_3

202 and presence of mineral dust in the atmosphere in North China, the calculated pH in aerosol

203 water is between 5.0 and 7.0 (Cao et al., 2013). The SO_2 uptake coefficient on aerosol water

204 surface is estimated to be about $10^{-4} \sim 10^{-5}$ if the sulfite oxidation is catalyzed by Fe^{3+}. The

205 sulfate heterogeneous formation from SO_2 is therefore parameterized as a first-order

206 irreversible uptake by aerosols, with a reactive uptake coefficient of 0.5×10^{-4}, assuming that

Atmospheric
Chemistry
and Physics
Discussions

207   there is enough alkalinity to maintain the high iron-catalyzed reaction rate:

208    $$\frac{d[SO_2]}{dt} = -\left(\frac{1}{4}\gamma_{SO_2}\upsilon_{SO_2}A_w\right)[SO_2]$$

209   where $[SO_2]$ is the SO_2 concentration, A_w is the aerosol water surface area, γ_{SO_2} is the SO_2

210   reactive uptake coefficient, and υ_{SO_2} is the SO_2 thermal velocity. Considering that O_3 and

211   NO_2 also play a considerable role in the sulfite oxidation when pH is high (Pandis and

212   Seinfeld, 1989), future studies are needed to consider the O_3 and NO_2 contribution to the

213   sulfate formation.

214   A box model is devised to interpret the rapid growth of sulfate observed at IEECAS

215   site during 2013 wintertime in Xi'an. In this model, the proposed heterogeneous reaction of

216   SO_2 involving aerosol water (hereafter referred to as $HRSO_2$) parameterization is included

217   and ISORROPIA (Version 1.7) is used to simulate sulfate, nitrate, ammonium aerosols, and

218   aerosol water. In addition, inorganic aerosols are represented by a two-moment modal

219   approach with a lognormal size distribution. A severe haze episode occurred from December

220   16 to 25, 2013 in GZB, with the average observed $[PM_{2.5}]$ exceeding 400 µg m^{-3} during the

221   period from December 23 to 25, 2013. The HR-ToF-AMS measured sulfate concentrations

222   reaching about 250 µg m^{-3} in the morning on December 23, and particularly, the observed

223   sulfate concentration increased from 132 µg m^{-3} at 07:30 BJT to 240 µg m^{-3} at 09:30 BJT.

224   The box model is utilized to simulate the rapid sulfate growth from 07:30 to 09:30 BJT,

225   constrained by the observed temperature, SO_2, nitrate, and ammonium (Table 2). There was

226   no RH observation at the IEECAS site; the observed RH at adjacent meteorological stations

227   ranged from 93% to 99% during the time period. In addition, the atmosphere was calm and

228   stable during the simulation period due to the control of a high pressure system over GZB, so

229   the horizontal transport is not considered. Various RHs from 93% to 99% are used to

230   calculate the sulfate growth in the box model. Figure 6 shows the calculated and observed

231   sulfate concentrations from 07:30 to 09:30 on December 23, 2013. The RH significantly

Atmospheric
Chemistry
and Physics
Discussions

232   influences the sulfate formation and the sulfate concentrations increase nonlinearly with the

233   RH. When the RH is 93%, the sulfate concentration is increased by 22.7 $\mu g\ m^{-3}$ after 2-hour

234   integration, whereas the enhanced sulfate concentration reaches 216.6 $\mu g\ m^{-3}$ when the RH is

235   99%. The simulated sulfate concentrations are best fit for the observation when the RH is

236   98%. It is worth noting that, when RH is high (i.e., exceeding 95% or so), there is always the

237   possibility of the presence of fog. Studies have demonstrated that for every observed sulfate

238   peak in the 1980s in Los Angeles, there is fog present (Pandis and Seinfeld, 1989; Pandis et

239   al., 1992). Hence, the box model simulations with the RH ranging from 93% to 99% strongly

240   suggest that there was at least some patchy fog in the area, which would provide sufficient

241   water for the rapid iron-catalyzed reaction. Further studies need to be performed to

242   investigate the possible contributions of the patchy fog on the sulfate formation.

243

244   **3.2   Sulfate Simulations in GZB and BTH**

245   The proposed $HRSO_2$ parameterization is further incorporated into the WRF-CHEM

246   model to simulate sulfate aerosols. Two simulations are performed for GZB and BTH

247   respectively, including the base case (hereafter referred to as B-case) without the $HRSO_2$

248   parameterization and the enhanced oxidation case (hereafter referred to as E-case) with the

249    $HRSO_2$ parameterization. In Figures 7 and 8, we present the spatial distributions of calculated

250   and observed near-surface [$PM_{2.5}$] at 00:00 BJT in the E-case on selected six days

251   representing the haze development in GZB and BTH, respectively, along with the simulated

252   wind fields. In general, the predicted $PM_{2.5}$ spatial patterns agree well with the observations

253   at the ambient monitoring sites in GZB and BTH. The model reproduces well the high [$PM_{2.5}$]

254   in GZB, although it tends to underestimate the observation in the west of GZB. Due to the

255   specific topography, when the northeast winds are prevalent in GZB, pollutants tend to

256   accumulate, and simulated and observed [$PM_{2.5}$] can be up to 500 $\mu g\ m^{-3}$. When the north

Atmospheric
Chemistry
and Physics
Discussions

257   winds are intensified on 26 December 2013, the pollutants commence to be transported

258   outside of GZB. In BTH, simulated weak winds cause severe $PM_{2.5}$ pollutions, with $[PM_{2.5}]$

259   frequently exceeding 250 µg m^{-3} at most of areas of BTH, which is consistent with the

260   observations over monitoring sites. Hence, in general, the model reasonably well reproduces

261   the haze formation in GZB and BTH.

262   In the present study, ISORROPIA (Version 1.7) is employed to predict the

263   thermodynamic equilibrium between the sulfate-nitrate-ammonium-water aerosols and their

264   gas phase precursors H_2SO_4-HNO_3-NH_3-water vapor. SO_2 and NO_2 are the precursors of

265   H_2SO_4 and HNO_3, so it is imperative to evaluate the SO_2 and NO_2 simulations using the

266   measurements to more reasonably calculate inorganic aerosols concentrations.

267   Figures 9 and 10 show the temporal profiles of observed and simulated near-surface

268    $[NO_2]$ and $[SO_2]$ averaged over monitoring sites in GZB from December 16 to 27, 2013 and

269   in BTH from January 13 to 21, 2014, respectively. The model performs well in simulating the

270    $[NO_2]$ temporal variations compared with observations in GZB and BTH, both with the *IOA*

271   of 0.91 in the E-case. The difference of the simulated $[NO_2]$ in the B-case and E-case is minor,

272   showing that the impact of the $HRSO_2$ parameterization on NO_2 simulations is not significant

273   in GZB and BTH. Although the model replicates the temporal variations of $[SO_2]$ compared

274   to the measurements in GZB and NCP in the E-case with *IOAs* of around 0.80, the model

275   biases still exist. The model generally underestimates $[SO_2]$ in GZB and BTH, with *MBs* of -

276   3.4 µg m^{-3} and -0.8 µg m^{-3}. One of the possible reasons for SO_2 simulation biases is that large

277   amounts of SO_2 are emitted from point sources, such as power plants or agglomerated

278   industrial zones, and the transport of SO_2 from point sources is more sensitive to the wind

279   field simulation uncertainties (Bei et al., 2012). The $HRSO_2$ parameterization generally

280   improves the SO_2 simulations by accelerating SO_2 conversions to sulfate, decreasing the *MB*

281   from 11.0 µg m^{-3} in the B-case to -3.4 µg m^{-3} in the E-case in GZB and 5.0 µg m^{-3} in the B-

Atmospheric
Chemistry
and Physics
Discussions

282   case to -0.8 µg m^{-3} in the E-case in BTH. Overall, the model performs well in simulating the

283   NO_2 and SO_2 temporal variations against the measurements in GZB and BTH in the E-case.

284   Figures 11 and 12 display the simulated and observed inorganic aerosol variations in

285   Xi'an from December 16 to 27, 2013 and in Beijing from January 13 to 21, 2014,

286   respectively. In Xi'an, the observed sulfate mass concentrations range from 50 to 250 µg m^{-3},

287   constituting the second most important $PM_{2.5}$ component during the episode. The $HRSO_2$

288   parameterization substantially improves the sulfate simulations in the E-case compared to

289   those in the B-case against the measurements. In the B-case, the sulfate concentrations are

290   remarkably underestimated, with a *MB* of -72.4 µg m^{-3} (Table 3). However, in the E-case, the

291   WRF-CHEM model generally yields the observed sulfate variations during the 11-day

292   episode, with a *MB* of -17.0 µg m^{-3} and an *IOA* of 0.89. It is worth noting that the model has

293   difficulties in reproducing the long-range transport sulfate contribution, and considerably

294   underestimates the observed sulfate mass concentration on December 17. The model also

295   cannot replicate the slow transition of synoptic situations on December 21, and the plume

296   formed in Xi'an is pushed to the northeast of Xi'an, causing underestimation of sulfate

297   aerosols (Bei et al., 2016).

298   In Beijing, the model also reproduces the observed sulfate variations reasonably well

299   during the 7-day episode in the E-case, with a *MB* of -0.8 µg m^{-3} and an *IOA* of 0.88 (Table

300   3), but cannot adequately predict the observed sulfate peaks. The high level of sulfate

301   aerosols in Beijing is generally determined by the transport from surrounding areas,

302   particularly from the regions in the south or east. Uncertainties of the timing, depth, and

303   intensity of the simulated southerly or easterly wind fronts significantly influence the model

304   performance. For example, the early occurrence of the southerly wind fronts causes an

305   overestimation of sulfate aerosols during the daytime on January 15. The model also fails to

306   produce the observed high sulfate mass concentration in the evening during January 17 due to

Atmospheric
Chemistry
and Physics
Discussions

Open Access

EGU

307   the simulated weak southerly or easterly wind fronts. The improvement of sulfate simulations

308   caused by the HRSO$_2$ parameterization in Beijing is not as obvious as that in Xi'an due to the

309   very humid conditions in GZB during the simulation period, which facilitate the rapid

310   conversion of SO$_2$ to sulfate and cause the SO$_2$ heterogeneous conversion to be the dominant

311   sulfate source.

312   Although the *IOA* for nitrate aerosols is 0.83, the nitrate underestimation is rather large

313   from 17 to 21 December 2013 in Xi'an in the E-case, caused by the model failure in

314   simulating the long-range transport of pollutants from the east outside of GZB. The nitrate

315   simulations are improved in Beijing compared to those in Xi'an, with a *MB* of -4.2 μg m^{-3}

316   and an *IOA* of 0.88 in the E-case. The nitrate simulations in the B-case are slightly better than

317   those in the E-case, caused by the underestimation of sulfate aerosols in the B-case, which is

318   favorable for more HNO$_3$ to exist in the aerosol phase. The model performs well in predicting

319   the ammonium aerosols in Xi'an and Beijing, with *IOAs* of around 0.90 in the E-case. The

320   ammonium simulations in the E-case are improved compared to those in the B-case against

321   the measurement, showing that sulfate aerosols play a more important role in the ammonium

322   aerosol formation. Considering the substantial influence of simulated meteorological fields

323   uncertainties on the aerosol species comparison at a single site (Bei et al., 2012), the HRSO$_2$

324   parameterization performs reasonably well in simulating the observed inorganic aerosol

325   variations in Xi'an and Beijing in the E-case.

326   Figure 13 presents the observed and simulated diurnal cycles of mass concentrations of

327   NO$_2$ and SO$_2$ averaged over GZB and BTH and the sulfate, nitrate, and ammonium aerosols

328   in Xi'an and Beijing during the simulated episodes. The WRF-CHEM model performs well

329   in simulating the NO$_2$ diurnal cycles compared to measurements over GZB and BTH in the

330   E-case. The model also reasonably reproduces the observed diurnal cycles of SO$_2$ over GZB,

331   sulfate, nitrate, and ammonium aerosols in Xi'an in the E-case, particularly the sulfate

332   simulations are significantly improved in the E-case compared with the B-case against the

333   measurements. However, the model does not predict well the observed diurnal cycles of

334   sulfate, nitrate, and ammonium aerosols in Beijing, showing the model biases in simulating

335   the south or east wind fronts.

336   As one of the most important components of PM$_{2.5}$, reasonable representation of sulfate

337   heterogeneous formation in CTMs is imperative to PM$_{2.5}$ simulations and predictions. Figure

338   14 presents the temporal profiles of observed and simulated near-surface [PM$_{2.5}$] averaged

339   over monitoring sites in GZB from December 16 to 27, 2013 and in BTH from January 13 to

340   21, 2014, respectively. Inclusion of the HRSO$_2$ parameterization in the E-case improves the

341   ability of the model to reproduce the PM$_{2.5}$ measurements in GZB and BTH. In GZB, due to

342   very humid conditions which facilitate the heterogeneous sulfate formation during the

343   episode, the simulated PM$_{2.5}$ mass concentrations are increased by more than 40 µg m^{-3} in the

344   E-case compared to the B-case, and more consistent with the measurements. The HRSO$_2$

345   parameterization also improves the PM$_{2.5}$ simulations in BTH, reducing the underestimation

346   from around -13.3 to -5.1 µg m^{-3}. The HRSO$_2$ parameterization enhances considerably the

347   [PM$_{2.5}$] in GZB (Figure 15), with the average [PM$_{2.5}$] contribution of about 10 – 50 µg m^{-3}

348   from December 16 to 27, 2013. The average [PM$_{2.5}$] contributions of the sulfate

349   heterogeneous formation is around 2 – 30 µg m^{-3} in BTH (Figure 15) from January 13 to 21,

350   2014, lower than those in GZB.

351   The sulfate aerosol significantly affects nitrate and ammonium formation in the

352   atmosphere due to its stability and the deliberate thermodynamic equilibrium between

353   inorganic aerosols and their precursors. The simulated hourly near-surface sulfate

354   concentrations in E-case during the whole episode are first subdivided into 20 bins with the

355   interval of 5 µg m^{-3}. Inorganic aerosols and PM$_{2.5}$ concentrations in the B-case and E-case as

356   the bin sulfate concentrations in the E-case following the grid cells are assembled

Atmospheric
Chemistry
and Physics
Discussions

357   respectively, and an average of inorganic aerosols and $PM_{2.5}$ concentrations in each bin are

358   calculated. Figures 16 and 17 show the impacts of the $HRSO_2$ parameterization on the

359   inorganic aerosols and $PM_{2.5}$ simulations in GZB and NCP, respectively. The heterogeneous

360   sulfate formation determines the sulfate level when the sulfate concentration in the E-case is

361   more than 25 $\mu g\ m^{-3}$, with the contribution exceeding 50% in GZB. However, in BTH, the

362   heterogeneous sulfate formation plays a more important role in the sulfate level only when

363   the sulfate concentration in the E-case exceeds 45 $\mu g\ m^{-3}$. If the $HRSO_2$ parameterization is

364   not considered, the model generally predicts more nitrate and less ammonium aerosols

365   (Figures 16b-c and 17b-c). In addition, the $[PM_{2.5}]$ contributions of the heterogeneous sulfate

366   formation exceed 5% and 10% when the simulated sulfate concentrations in the E-case are

367   more than 10 $\mu g\ m^{-3}$ and 80 $\mu g\ m^{-3}$ in GZB respectively (Figure 16d). However, in BTH, the

368   contributions exceed 5% when the simulated sulfate concentrations in the E-case are higher

369   than 50 $\mu g\ m^{-3}$ (Figure 17d).

370

371   **4   Summary and Conclusions**

372   In the present study, a parameterization of sulfate heterogeneous formation involving

373   aerosol water ($HRSO_2$) is developed based on the daily filter measurements in Xi'an since

374   2003. A SO_2 heterogeneous reaction parameterization has been proposed, in which the SO_2

375   oxidation in aerosol water by O_2 catalyzed by Fe^{3+} is limited by mass transfer resistances in

376   the gas-phase and the gas-particle interface. The sulfate heterogeneous formation from SO_2 is

377   parameterized as a first-order irreversible uptake by aerosol water surfaces, with a reactive

378   uptake coefficient of 0.5×10^{-4} assuming that there is enough alkalinity to maintain the high

379   iron-catalyzed reaction rate. A box model with the $HRSO_2$ parameterization successfully

380   reproduces the observed rapid sulfate formation at IEECAS site in Xi'an.

381   The $HRSO_2$ parameterization is implemented into the WRF-CHEM model to simulate

Atmospheric
Chemistry
and Physics
Discussions

382   sulfate aerosols. Two persistent heavy haze pollution episodes are simulated with and without

383   the SO_2 heterogeneous reaction: (1) December 16 to 27, 2013 in GZB, and (2) January 13 to

384   21, 2014 in BTH. In general, the model performs reasonably well in simulating the $PM_{2.5}$

385   distributions, the NO_2 and SO_2 temporal variations compared with observations in GZB and

386   NCP. The $HRSO_2$ parameterization improves the SO_2 simulations by accelerating SO_2

387   conversions to sulfate aerosols.

388   The $HRSO_2$ parameterization substantially improves the sulfate simulations compared

389   to the measurements in Xi'an and Beijing, particularly under humid conditions. In Xi'an, the

390   sulfate concentrations are substantially underestimated when the $HRSO_2$ parameterization is

391   not considered in the simulations. Inclusion of the $HRSO_2$ parameterization significantly

392   enhances the sulfate formation, and the model generally produces the observed sulfate

393   variations during the 11-day episode. In Beijing, improvement in sulfate simulations with

394    $HRSO_2$ parameterization is not as obvious as that in Xi'an because of the very humid

395   conditions in GZB during the simulation period. The $HRSO_2$ parameterization also improves

396   the ammonium simulations in Xi'an and Beijing compared to observations, as well as

397   appreciably improves the $PM_{2.5}$ simulations against the measurements over monitoring sites

398   in GZB and NCP.

399   In summary, reasonable representation of sulfate heterogeneous formation not only

400   improves the $PM_{2.5}$ simulations, but also helps rationally verify the contribution of inorganic

401   aerosols to $PM_{2.5}$, providing the underlying basis for better understanding the haze formation

402   and supporting the design and implementation of emission control strategies.

403

404   Data availability: The real-time NO_2, SO_2 and $PM_{2.5}$ are accessible for the public on the

405   website http://106.37.208.233:20035/. The historic profile of observed ambient pollutants is

406   also available at http://www.aqistudy.cn/.

413
414
415
416

Atmospheric
Chemistry
and Physics
Discussions

Open Access

417   **References**

418   Alexander, B., Park, R. J., Jacob, D. J., and Gong, S. L.: Transition metal-catalyzed oxidation
419   of atmospheric sulfur: Global implications for the sulfur budget, Journal of Geophysical
420   Research-Atmospheres, 114, 13, 10.1029/2008jd010486, 2009.

421   Barrie, L. A., Yi, Y., Leaitch, W. R., Lohmann, U., Kasibhatla, P., Roelofs, G. J., Wilson, J.,
422   McGovern, F., Benkovitz, C., Melieres, M. A., Law, K., Prospero, J., Kritz, M.,
423   Bergmann, D., Bridgeman, C., Chin, M., Christensen, J., Easter, R., Feichter, J., Land, C.,
424   Jeuken, A., Kjellstrom, E., Koch, D., and Rasch, P.: A comparison of large-scale
425   atmospheric sulphate aerosol models (COSAM): overview and highlights, Tellus Series
426   B-Chemical and Physical Meteorology, 53, 615-645, 10.1034/j.1600-0889.2001.530507.x,
427   2001.

428   Bei, N., Li, G., and Molina, L. T.: Uncertainties in SOA simulations due to meteorological
429   uncertainties in Mexico City during MILAGRO-2006 field campaign, Atmospheric
430   Chemistry and Physics, 12, 11295-11308, 10.5194/acp-12-11295-2012, 2012.

431   Bei, N. F., Li, G. H., Huang, R. J., Cao, J. J., Meng, N., Feng, T., Liu, S. X., Zhang, T.,
432   Zhang, Q., and Molina, L. T.: Typical synoptic situations and their impacts on the
433   wintertime air pollution in the Guanzhong basin, China, Atmospheric Chemistry and
434   Physics, 16, 7373-7387, 10.5194/acp-16-7373-2016, 2016.

435   Cao, J., Tie, X., Dabberdt, W. F., Jie, T., Zhao, Z., An, Z., and Shen, Z.: On the potential high
436   acid deposition in northeastern China, Journal of Geophysical Research-Atmospheres,
437   118, 4834-4846, doi:10.1002/jgrd.50381, 2013.

438   Chen, F., and Dudhia, J.: Coupling an advanced land surface-hydrology model with the Penn
439   State-NCAR MM5 modeling system. Part I: Model implementation and sensitivity, Mon.
440   Weather Rev., 129, 569-585, 10.1175/1520-0493(2001)129<0569:caalsh>2.0.co;2, 2001.

441   Chen, W., Yan, L., and Zhao, H. M.: Seasonal Variations of Atmospheric Pollution and Air
442   Elser, M., Huang, R.-J., Wolf, R., Slowik, J. G., Wang, Q., Canonaco, F., Li, G., Bozzetti,
443   C., Daellenbach, K. R., Huang, Y., Zhang, R., Li, Z., Cao, J., Baltensperger, U., El-
444   Haddad, I., and Prévôt, A. S. H.: New insights into $PM_{2.5}$ chemical composition and
445   sources in two major cities in China during extreme haze events using aerosol mass
446   spectrometry, Atmospheric Chemistry and Physics, 16, 3207-3225, doi:10.5194/acp-16-
447   3207-2016, 2016.

448   Chou, M.-D. and M. J. Suarez: A solar radiation parameterization for atmospheric studies,
449   NASA Tech. Rep. NASA/TM-1999-10460, 15, 38 pp, 1999.

450   Chou, M.-D. and M. J. Suarez: A thermal infrared radiation parameterization for atmospheric
451   studies, NASA/TM-2001-104606, 19, 55 pp, 2001.

452   Feichter, J., Kjellstrom, E., Rodhe, H., Dentener, F., Lelieveld, J., and Roelofs, G. J.:
453   Simulation of the tropospheric sulfur cycle in a global climate model, Atmospheric
454   Environment, 30, 1693-1707, 10.1016/1352-2310(95)00394-0, 1996.

455   Gerhardsson, L., Oskarsson, A., and Skerfving, S.: Acid precipitation effects on trace-
456   elements and human health, Science of Total Environment, 153, 237-245, 10.1016/0048-
457   9697(94)90203-8, 1994.

458   Grell, G., and Baklanov, A.: Integrated modeling for forecasting weather and air quality: A
459   call for fully coupled approaches, Atmospheric Environment, 45, 6845-6851,
460   10.1016/j.atmosenv.2011.01.017, 2011.

Atmospheric
Chemistry
and Physics
Discussions

461 Guo, S., Hu, M., Zamora, M. L., Peng, J. F., Shang, D. J., Zheng, J., Du, Z. F., Wu, Z., Shao,
462   M., Zeng, L. M., Molina, M. J., and Zhang, R. Y.: Elucidating severe urban haze
463   formation in China, Proceedings of the National Academy of Sciences of the United
464   States of America, 111, 17373-17378, 10.1073/pnas.1419604111, 2014.

465 Guenther, A., Karl, T., Harley, P., Wiedinmyer, C., Palmer, P. I., and Geron, C.: Estimates of
466   global terrestrial isoprene emissions using MEGAN (Model of Emissions of Gases and
467   Aerosols from Nature), Atmospheric Chemistry and Physics, 6, 3181-3210, 2006.

468 Harris, E., Sinha, B., van Pinxteren, D., Tilgner, A., Fomba, K. W., Schneider, J., Roth, A.,
469   Gnauk, T., Fahlbusch, B., Mertes, S., Lee, T., Collett, J., Foley, S., Borrmann, S., Hoppe,
470   P., and Herrmann, H.: Enhanced role of transition metal ion catalysis during in-cloud
471   oxidation of SO_2, Science, 340, 2013.

472 He, H., Wang, Y. S., Ma, Q. X., Ma, J. Z., Chu, B. W., Ji, D. S., Tang, G. Q., Liu, C., Zhang,
473   H. X., and Hao, J. M.: Mineral dust and NO_x promote the conversion of SO_2 to sulfate in
474   heavy pollution days, Scientific Report, 4, 5, 10.1038/srep04172, 2014.

475 Hong, S.-Y., and Lim, J.-O. J.: The WRF Single-Moment 6-Class Microphysics Scheme
476   (WSM6), Asia-Pacific Journal of Atmospheric Sciences, 42, 129-151, 2006.

477 Horowitz, L. W., Walters, S., Mauzerall, D. L., Emmons, L. K., Rasch, P. J., Granier, C., Tie,
478   X. X., Lamarque, J. F., Schultz, M. G., Tyndall, G. S., Orlando, J. J., and Brasseur, G. P.:
479   A global simulation of tropospheric ozone and related tracers: Description and evaluation
480   of MOZART, version 2, Journal of Geophysical Research-Atmospheres, 108, 29,
481   10.1029/2002jd002853, 2003.

482 Jacob, D. J., and Hoffmann, M. R.: A dynamic model for the production of H^+, NO_3^-, and
483   SO_4^{2-} in urban fog, Journal of Geophysical Research-Oceans and Atmospheres, 88, 6611-
484   6621, 10.1029/JC088iC11p06611, 1983.

485 Jacob, D. J., Waldman, J. M., Munger, J. W., and Hoffmann, M. R.: A field investigation of
486   physical and chemical mechanisms affecting pollutant concentrations in fog droplets,
487   Tellus Series B-Chemical and Physical Meteorology, 36, 272-285, 1984.

488 Jacob, D. J., Gottlieb, E. W., and Prather, M. J.: Chemistry of a polluted cloudy boundary-
489   layer, Journal of Geophysical Research-Atmospheres, 94, 12975-13002,
490   10.1029/JD094iD10p12975, 1989.

491 Janjić, Z. I.: Nonsingular Implementation of the Mellor–Yamada Level 2.5 Scheme in the
492   NCEP Meso Model, Ncep Office Note, 436, 2002.

493 Kasibhatla, P., Chameides, W. L., and StJohn, J.: A three-dimensional global model
494   investigation of seasonal variations in the atmospheric burden of anthropogenic sulfate
495   aerosols, Journal of Geophysical Research-Atmospheres, 102, 3737-3759,
496   10.1029/96jd03084, 1997.

497 Kawamoto, K., Hayasaka, T., Uno, I., and Ohara, T.: A correlative study on the relationship
498   between modeled anthropogenic aerosol concentration and satellite-observed cloud
499   properties over east Asia, Journal of Geophysical Research-Atmospheres, 111, 7,
500   10.1029/2005jd006919, 2006.

501 Laskin, A., Gaspar, D. J., Wang, W. H., Hunt, S. W., Cowin, J. P., Colson, S. D., and
502   Finlayson-Pitts, B. J.: Reactions at interfaces as a source of sulfate formation in sea-salt
503   particles, Science, 301, 340-344, 10.1126/science.1085374, 2003.

Atmospheric
Chemistry
and Physics
Discussions

504   Li, G., Zhang, R., Fan, J., and Tie, X.: Impacts of black carbon aerosol on photolysis and
505   ozone, Journal of Geophysical Research, 110, 10.1029/2005jd005898, 2005.

506   Li, G., Lei, W., Zavala, M., Volkamer, R., Dusanter, S., Stevens, P., and Molina, L. T.:
507   Impacts of HONO sources on the photochemistry in Mexico City during the MCMA-
508   2006/MILAGO Campaign, Atmospheric Chemistry and Physics, 10, 6551-6567,
509   10.5194/acp-10-6551-2010, 2010.

510   Li, G., Bei, N., Tie, X., and Molina, L. T.: Aerosol effects on the photochemistry in Mexico
511   City during MCMA-2006/MILAGRO campaign, Atmospheric Chemistry and Physics, 11,
512   5169-5182, 10.5194/acp-11-5169-2011, 2011a.

513   Li, G., Zavala, M., Lei, W., Tsimpidi, A. P., Karydis, V. A., Pandis, S. N., Canagaratna, M.
514   R., and Molina, L. T.: Simulations of organic aerosol concentrations in Mexico City using
515   the WRF-CHEM model during the MCMA-2006/MILAGRO campaign, Atmospheric
516   Chemistry and Physics, 11, 3789-3809, 10.5194/acp-11-3789-2011, 2011b.

517   Li, G., Lei, W., Bei, N., and Molina, L. T.: Contribution of garbage burning to chloride and
518        $PM_{2.5}$ in Mexico City, Atmospheric Chemistry and Physics, 12, 8751-8761, 10.5194/acp-
519   12-8751-2012, 2012.

520   Martin, L. R., and Hill, M. W.: The effect of ionic-strength on the manganese catalyzed
521   oxidation of sulfur(iv), Atmospheric Environment, 21, 2267-2270, 1987.

522   Mauldin, R. L., Berndt, T., Sipila, M., Paasonen, P., Petaja, T., Kim, S., Kurten, T.,
523   Stratmann, F., Kerminen, V. M., and Kulmala, M.: A new atmospherically relevant
524   oxidant of sulphur dioxide, Nature, 488, 193-196, 10.1038/nature11278, 2012.

525   Nakajima, T., Higurashi, A., Kawamoto, K., and Penner, J. E.: A possible correlation
526   between satellite-derived cloud and aerosol microphysical parameters, Geophysical
527   Research Letters, 28, 1171-1174, 10.1029/2000gl012186, 2001.

528   Nenes, A., Pandis, S. N., and Pilinis, C.: ISORROPIA: A new thermodynamic equilibrium
529   model for multiphase multicomponent inorganic aerosols, Aquatic Geochemistry, 4, 123-
530   152, 10.1023/a:1009604003981, 1998.

531   Pandis, S. N. and Seinfeld, J. H.: Mathematical modeling of acid deposition due to radiation
532   fog, Journal of Geophysical Research, 94, 12911-12923, 1989.

533   Pandis, S. N., Seinfeld, J. H., and Pilinis, C.: Heterogeneous sulfate production in an urban
534   fog, Atmospheric Environment Part a-General Topics, 26, 2509-2522, 10.1016/0960-
535   1686(92)90103-r, 1992.

536   Seinfeld, J. H. and Pandis, S. N.: Atmospheric Chemistry and Physics: From Air Pollution to
537   Climate Change, 2nd Edn., John Wiley & Sons Inc., New York, 2006.

538   Schindler, D. W.: Effects of acid-rain on fresh-water ecosystems, Science, 239, 149-157,
539   10.1126/science.239.4836.149, 1988.

540   Sun, Y., Wang, Z., Fu, P., Jiang, Q., Yang, T., Li, J., and Ge, X.: The impact of relative
541   humidity on aerosol composition and evolution processes during wintertime in Beijing,
542   China, Atmospheric Environment, 77, 927-934, 2013.

543   Tian, S. L., Pan, Y. P., and Wang, Y. S.: Size-resolved source apportionment of particulate
544   matter in urban Beijing during haze and non-haze episodes, Atmospheric Chemistry and
545   Physics, 16, 1-19, 10.5194/acp-16-1-2016, 2016.

546   Wang, X. F., Wang, W. X., Yang, L. X., Gao, X. M., Nie, W., Yu, Y. C., Xu, P., Zhou, Y.,
547   and Wang, Z.: The secondary formation of inorganic aerosols in the droplet mode through

548   heterogeneous aqueous reactions under haze conditions, Atmospheric Environment, 63,
549   68-76, 10.1016/j.atmosenv.2012.09.029, 2012.

550   Wang, Y. X., Zhang, Q. Q., Jiang, J. K., Zhou, W., Wang, B. Y., He, K. B., Duan, F. K.,
551   Zhang, Q., Philip, S., and Xie, Y. Y.: Enhanced sulfate formation during China's severe
552   winter haze episode in January 2013 missing from current models, Journal of
553   Geophysical Research-Atmospheres, 119, 16, 10.1002/2013jd021426, 2014.

554   Wesely, M. L.: Parameterization of surface resistances to gaseous dry deposition in regional-
555   scale numerical models, Atmospheric Environment, 23, 1293-1304,
556   http://dx.doi.org/10.1016/0004-6981(89)90153-4, 1989.

557   Worsnop, D. R., Zahniser, M. S., Kolb, C. E., Gardner, J. A., Watson, L. R., Vandoren, J. M.,
558   Jayne, J. T., and Davidovits, P.: Temperature-dependence of mass accommodation of SO_2
559   and H_2O_2 on aqueous surfaces, Journal of Physical Chemistry, 93, 1159-1172,
560   10.1021/j100340a027, 1989.

561   Xie, Y. N., Ding, A. J., Nie, W., Mao, H. T., Qi, X. M., Huang, X., Xu, Z., Kerminen, V. M.,
562   Petaja, T., Chi, X. G., Virkkula, A., Boy, M., Xue, L. K., Guo, J., Sun, J. N., Yang, X. Q.,
563   Kulmala, M., and Fu, C. B.: Enhanced sulfate formation by nitrogen dioxide:
564   Implications from in situ observations at the SORPES station, Journal of Geophysical
565   Research-Atmospheres, 120, 12679-12694, 10.1002/2015jd023607, 2015.

566   Xue, J., Yuan, Z., Griffith, S. M., Yu, X., Lau, A. K. H., and Yu, J. Z.: Sulfate Formation
567   Enhanced by a Cocktail of High NOx, SO2, Particulate Matter, and Droplet pH during
568   Haze-Fog Events in Megacities in China: An Observation-Based Modeling Investigation,
569   Environmental Science & Technology, 50(14), 7325-7334, 2016.

570   Zheng, G. J., Duan, F. K., Su, H., Ma, Y. L., Cheng, Y., Zheng, B., Zhang, Q., Huang, T.,
571   Kimoto, T., Chang, D., Pöschl, U., Cheng, Y. F., and He, K. B.: Exploring the severe
572   winter haze in Beijing: the impact of synoptic weather, regional transport and
573   heterogeneous reactions, Atmospheric Chemistry and Physics, 15, 2969-2983, 2015.

574   Zhang, Q., Streets, D. G., Carmichael, G. R., He, K. B., Huo, H., Kannari, A., Klimont, Z.,
575   Park, I. S., Reddy, S., Fu, J. S., Chen, D., Duan, L., Lei, Y., Wang, L. T., and Yao, Z. L.:
576   Asian emissions in 2006 for the NASA INTEX-B mission, Atmospheric Chemistry and
577   Physics, 9, 5131-5153, 2009.

578   Zhang, R. Y., Wang, G. H., Guo, S., Zarnora, M. L., Ying, Q., Lin, Y., Wang, W. G., Hu, M.,
579   and Wang, Y.: Formation of Urban Fine Particulate Matter, Chemical Reviews, 115,
580   3803-3855, 10.1021/acs.chemrev.5b00067, 2015.

581
582
583
584

Atmospheric
Chemistry
and Physics
Discussions

Open Access

Figure Captions

585

586   Figure 1 WRF-CHEM simulation domains with topography for (a) the Guanzhong basin and
587   (b) Beijing-Tianjin-Hebei. The black squares represent ambient monitoring sites. The
588   red filled circles in (a) and (b) denote the deployment locations of the HR-ToF-AMS
589   in Xi'an and Beijing, respectively.

590   Figure 2 Scatter plot of the observed sulfate with $PM_{2.5}$ mass concentrations at IEECAS site
591   in Xi'an during the wintertime from 2003 to 2011.

592   Figure 3 Average O_3 mass concentrations over monitoring sites in GZB as a function of the
593        $PM_{2.5}$ mass concentration during the wintertime from 2013 to 2015.

594   Figure 4 Scatter plot of the observed relative humidity with sulfate mass concentrations at
595   IEECAS site in Xi'an during the wintertime from 2003 to 2011.

596   Figure 5 Scatter plot of the observed $PM_{2.5}$ with iron mass concentrations at IEECAS site in
597   Xi'an during the wintertime from 2003 to 2011.

598   Figure 6 Sulfate growth simulated by the box model with the $HRSO_2$ parameterization under
599   various relative humidity conditions at IEECAS site in Xi'an from 07:30 to 09:30 BJT
600   on December 23, 2013. The black dots denote the HR-ToF-AMS measurement and
601   the solid lines with different colors represent the box model simulations under
602   different relative humidity.

603   Figure 7 Pattern comparison of simulated vs. observed near-surface $PM_{2.5}$ at 00:00 BJT
604   during the selected six days in GZB from 16 to 27 December 2013. Colored circles:
605        $PM_{2.5}$ observations; color contour: $PM_{2.5}$ simulations in the E-case; black arrows:
606   simulated surface winds in the E-case.

607   Figure 8 Same as Figure 7, but in BTH from 13 to 21 January 2014.

608   Figure 9 Comparison of measured and predicted diurnal profiles of near-surface hourly (a)
609   NO_2 and (b) SO_2 averaged over all ambient monitoring sites in GZB from 16 to 27
610   December 2013. The black dots correspond to the observations, and the solid red and
611   blue lines are the simulations in the E-case and B-case, respectively.

612   Figure 10 Same as Figure 9, but in BTH from 13 to 21 January 2014.

613   Figure 11 Comparison of measured and simulated diurnal profiles of inorganic aerosols of (a)
614   sulfate, (b) nitrate, and (c) ammonium in Xi'an from 16 to 27 December 2013. The
615   black dots represent the observations, and the solid red and blue lines denote the
616   simulations in the E-case and B-case, respectively.

617   Figure 12 Same as Figure 11, but in Beijing from 13 to 21 January 2014.

618   Figure 13 Observed and simulated diurnal cycles of mass concentrations of NO_2 and SO_2
619   averaged over GZB and BTH and the sulfate, nitrate, and ammonium aerosols in
620   Xi'an and Beijing during the simulated episodes.

621   Figure 14 Comparison of measured and predicted diurnal profiles of near-surface hourly
622        $PM_{2.5}$ mass concentration averaged over all ambient monitoring stations (a) in GZB

623   from 16 to 27 December 2013 and (b) in BTH from 13 to 21 January 2014. The black
624   dots represent the observations, and the solid red and blue lines are the simulations in
625   the E-case and B-case, respectively.

626 Figure 15 Distribution of the average near-surface $PM_{2.5}$ contribution due to the SO_2
627   heterogeneous reactions in GZB and BTH during the simulated episodes.

628 Figure 16 Average (a) sulfate, (b) nitrate, (c) ammonium, and (d) $PM_{2.5}$ mass concentrations
629   in GZB during the simulation period as a function of the sulfate mass concentration in
630   the E-case. The red and blue dots represent average mass concentrations in the E-case
631   and B-case, respectively.

632 Figure 17 Same as Figure 16, but in BTH from 13 to 21 January 2014.

633

634

635

636

Atmospheric
Chemistry
and Physics
Discussions

637   Table 1 WRF-CHEM model configurations and observation sites
638

Regions	Guanzhong Basin (GZB)	Beijing-Tianjin-Hebei (BTH)
Simulation period	December 16 to 27, 2013	January 13 to 21, 2014
Domain size	150 × 150	
Domain center	34.25°N, 109°E	39°N, 117°E
Horizontal resolution	6km × 6km	
Vertical resolution	35 vertical levels with a stretched vertical grid with spacing ranging from 30 m near the surface, to 500 m at 2.5 km and 1 km above 14 km	
Microphysics scheme	WSM 6-class graupel scheme (Hong and Lim, 2006)	
Boundary layer scheme	MYJ TKE scheme (Janjić, 2002)	
Surface layer scheme	MYJ surface scheme (Janjić, 2002)	
Land-surface scheme	Unified Noah land-surface model (Chen and Dudhia, 2001)	
Longwave radiation scheme	Goddard longwave scheme (Chou and Suarez, 2001)	
Shortwave radiation scheme	Goddard shortwave scheme (Chou and Suarez, 1999)	
Meteorological boundary and initial conditions	NCEP 1°×1° reanalysis data	
Chemical initial and boundary conditions	MOZART 6-hour output (Horowitz et al., 2003)	
Anthropogenic emission inventory	Developed by Zhang et al. (2009)	
Biogenic emission inventory	MEGAN model developed by Guenther et al. (2006)	
Aerosol Observation Sites		
City	Xi'an	Beijing
Longitude and latitude	34.23°N, 108.88°E	40.00°N, 116.38°E

639
640
641
642

Atmospheric
Chemistry
and Physics

Discussions

Open Access

643 Table 2 Box model configurations

644

Time (BJT)	07:00 – 08:00	08:00 – 09:00	09:00 – 10:00
Temperature (^{o}C)	-3.7	-3.2	-2.1
SO_2 concentration ($\mu g\ m^{-3}$)	10.7	10.4	25.5
Nitrate concentration ($\mu g\ m^{-3}$)[*]	67.6	70.1	69.1
Ammonium concentration ($\mu g\ m^{-3}$)[*]	65.2	76.0	91.9

645 [*]The HR-ToF-AMS measures sulfate, nitrate, and ammonium aerosols with a time resolution of 1 minute. The
646 high temporal resolution nitrate and ammonium are used to constrain the box model and the hourly average is
647 presented in the table.

648

649

650

651

Atmospheric
Chemistry
and Physics
Discussions

Open Access

652 Table 3 Statistical comparisons of simulated and measured sulfate, nitrate, and ammonium
653 concentrations in Xi'an and Beijing

City	Species	E-case		B-case	
		MB (µg m^{-3})	IOA	MB (µg m^{-3})	IOA
Xi'an	Sulfate	-17.0	0.89	-72.4	0.50
	Nitrate	-13.4	0.83	-6.3	0.86
	Ammonium	-5.1	0.92	-20.1	0.72
Beijing	Sulfate	-0.8	0.88	-8.4	0.65
	Nitrate	-4.2	0.88	-1.9	0.92
	Ammonium	-2.7	0.89	-4.1	0.87
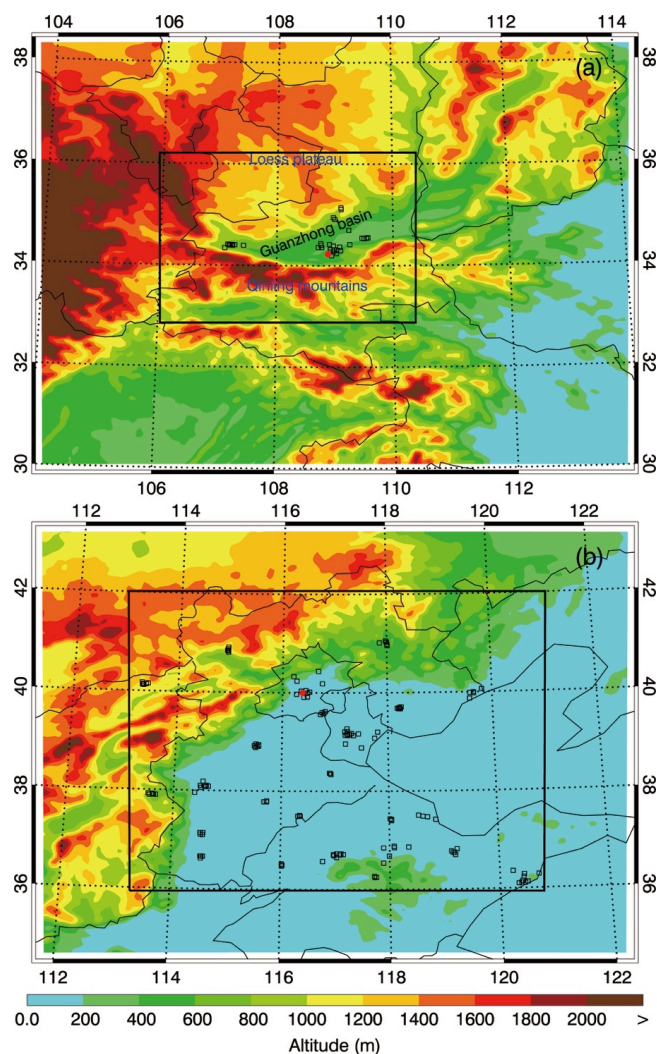
Atmospheric
Chemistry
and Physics
Discussions

667
668
669   Figure 1 WRF-CHEM simulation domains with topography for (a) the Guanzhong basin and
670   (b) Beijing-Tianjin-Hebei. The black squares represent ambient monitoring sites. The red
671   filled circles in (a) and (b) denote the deployment locations of the HR-ToF-AMS in Xi'an
672   and Beijing, respectively.
673
674
675
676

Atmospheric
Chemistry
and Physics
Discussions

Open Access
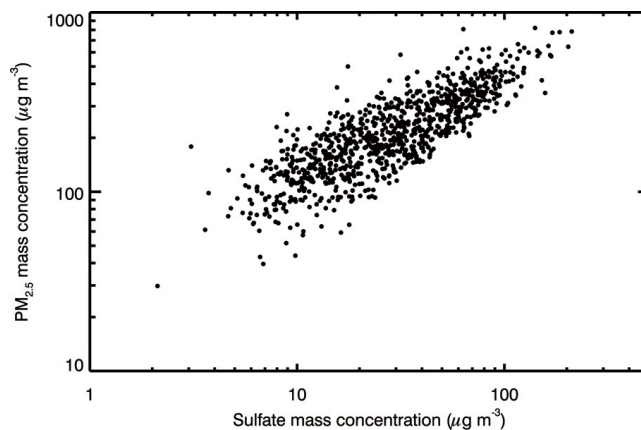
677
678
679 Figure 2 Scatter plot of the observed sulfate with PM$_{2.5}$ mass concentrations at IEECAS site
680 in Xi'an during the wintertime from 2003 to 2011.
681
682
683
684

Atmospheric
Chemistry
and Physics
Discussions

Open Access
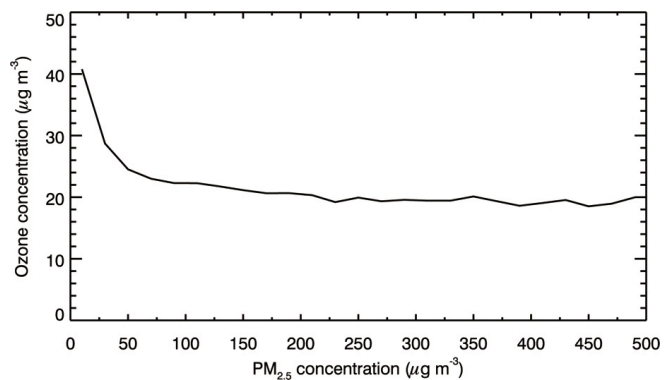
685
686
687   Figure 3 Average O_3 mass concentrations over monitoring sites in GZB as a function of the
688    $PM_{2.5}$ mass concentration during the wintertime from 2013 to 2015.
689
690
691
692

Atmospheric
Chemistry
and Physics
Discussions
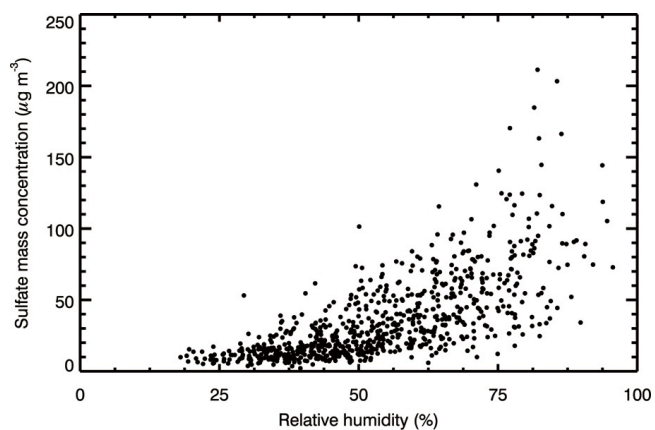
693
694
695   Figure 4 Scatter plot of the observed relative humidity with sulfate mass concentrations at
696   IEECAS site in Xi'an during the wintertime from 2003 to 2011.
697
698
699
700

Atmospheric
Chemistry
and Physics
Discussions

Open Access
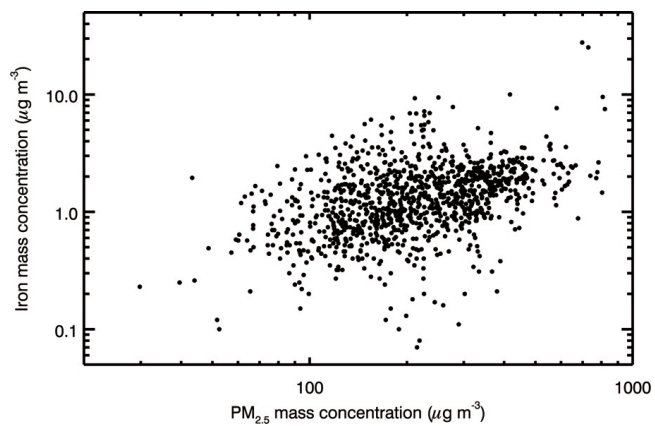
701
702
703   Figure 5 Scatter plot of the observed $PM_{2.5}$ with iron mass concentrations at IEECAS site in
704   Xi'an during the wintertime from 2003 to 2011.
705
706
707
708

Atmospheric
Chemistry
and Physics
Discussions

Open Access

EGU
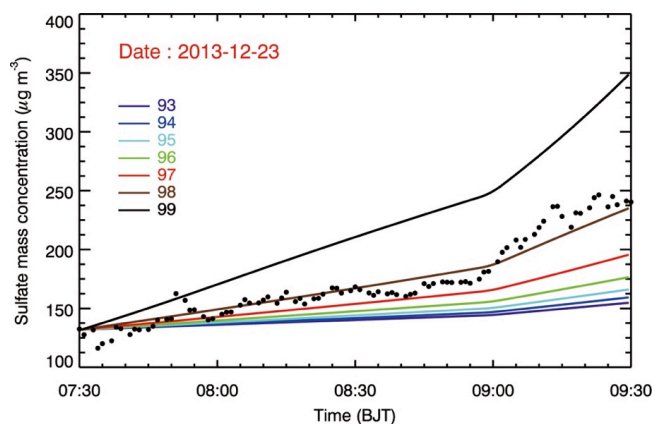
709
710
711   Figure 6 Sulfate growth simulated by the box model with the HRSO$_2$ parameterization under
712   various relative humidity at IEECAS site in Xi'an from 07:30 to 09:30 BJT on December 23,
713   2013. The black dots denote the HR-ToF-AMS measurement and the solid lines with
714   different colors represent the box model simulations under different relative humidity.
715
716
717
718
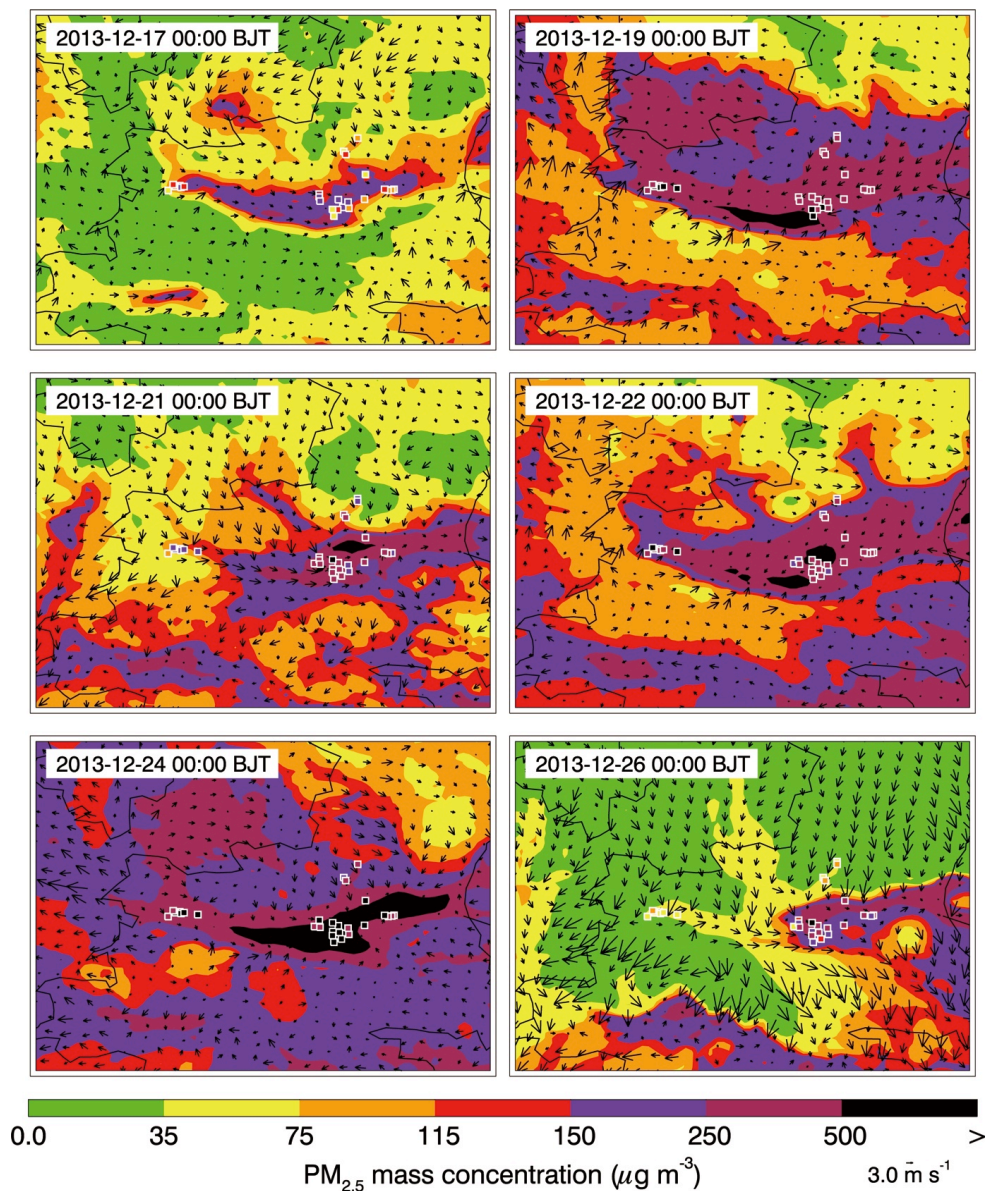
Figure 7 Pattern comparison of simulated vs. observed near-surface PM$_{2.5}$ at 00:00 BJT on
the selected six days in GZB from 16 to 27 December 2013. Colored circles: PM$_{2.5}$
observations; color contour: PM$_{2.5}$ simulations in the E-case; black arrows: simulated surface
winds in the E-case.
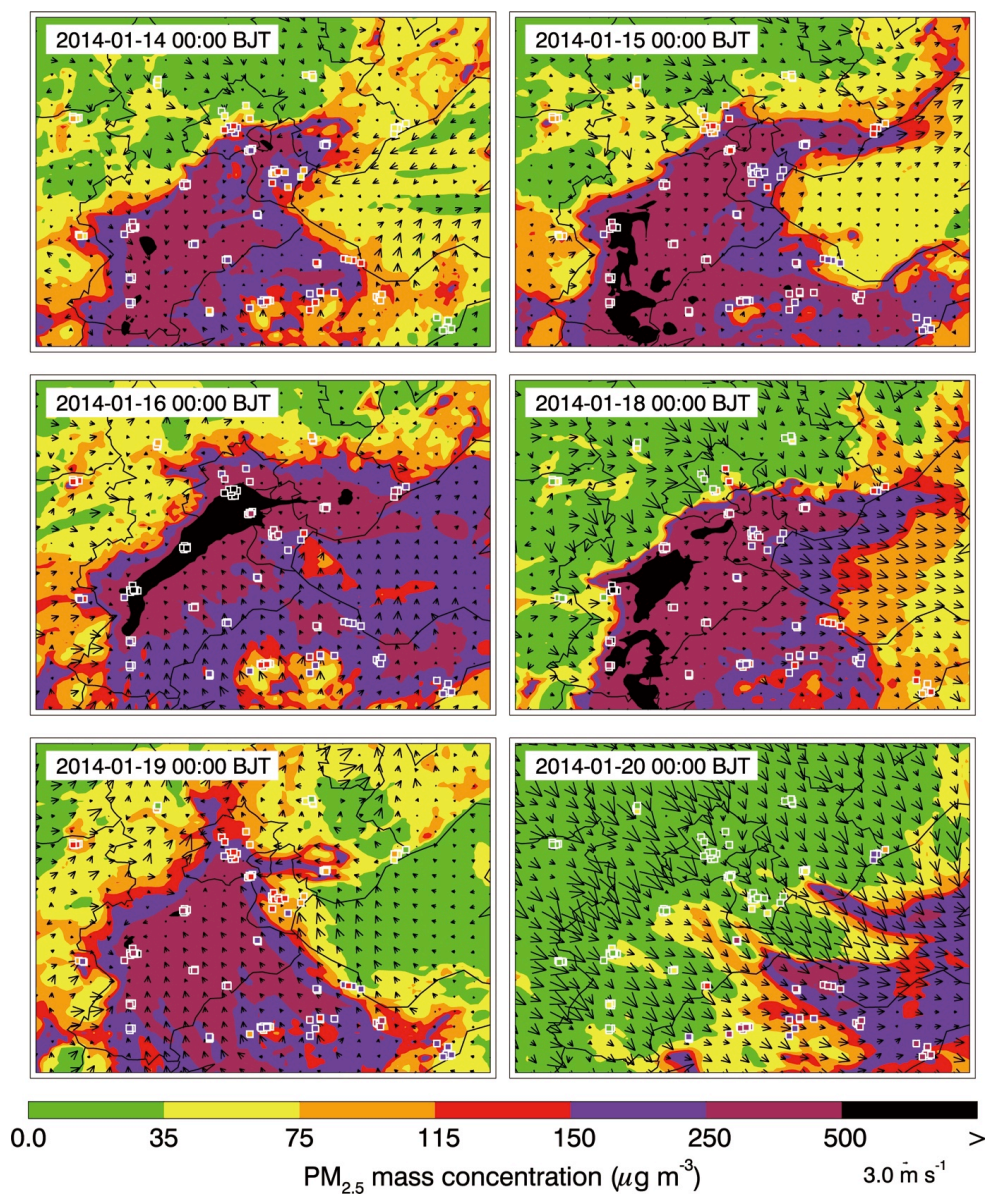
Figure 8 Same as Figure 7, but in BTH from 13 to 21 January 2014.
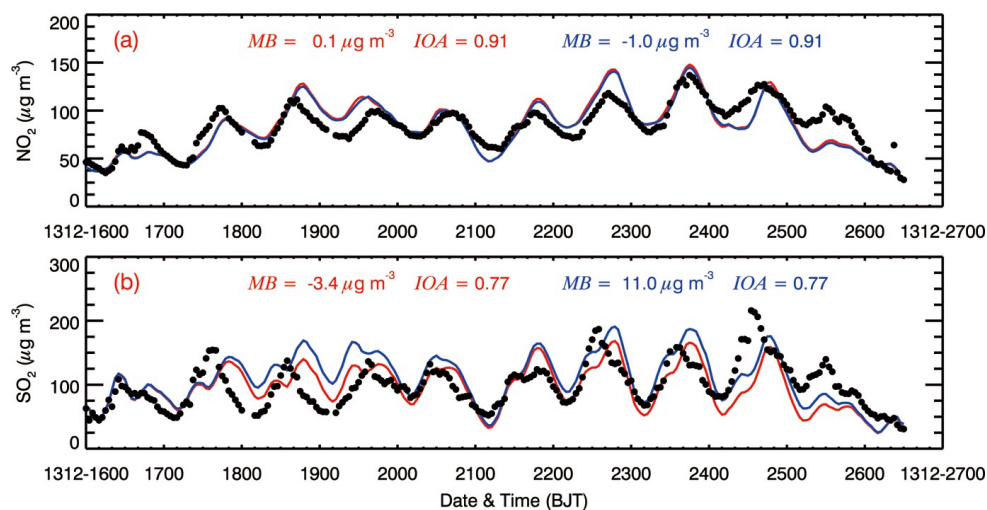
736
737
738   Figure 9 Comparison of measured and predicted diurnal profiles of near-surface hourly (a)
739   NO$_2$ and (b) SO$_2$ averaged over all ambient monitoring sites in GZB from 16 to 27 December
740   2013. The black dots correspond to the observations, and the solid red and blue lines are the
741   simulations in the E-case and B-case, respectively. The x-axis labels (named date and time)
742   represent year, month, day and hour (YYMM-DDHH) or day and hour (DDHH). For example, 1312-
743   1600 represents 00 BJT on 16 December 2013.
744
745
746
747
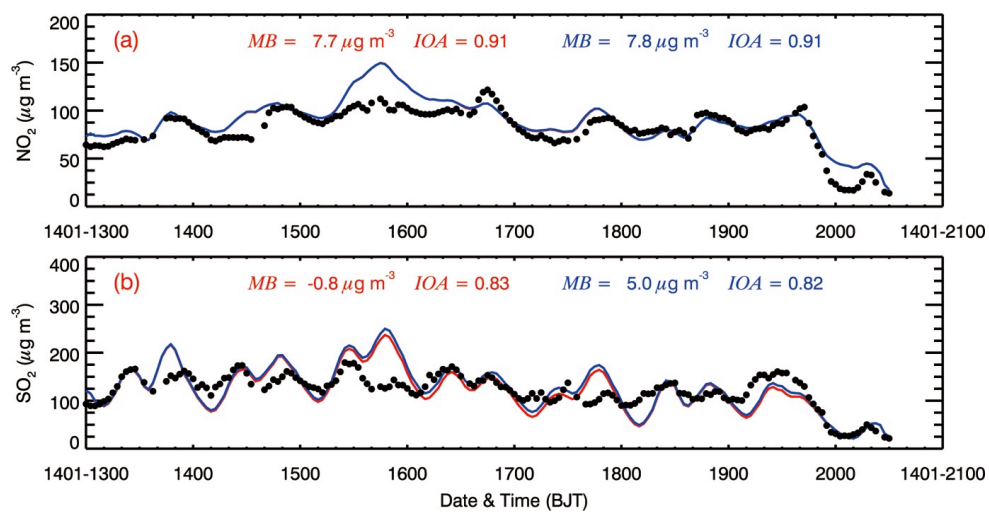
748
749
750   Figure 10 Same as Figure 9, but in BTH from 13 to 21 January 2014.
751
752
753
754

Atmospheric
Chemistry
and Physics
Discussions
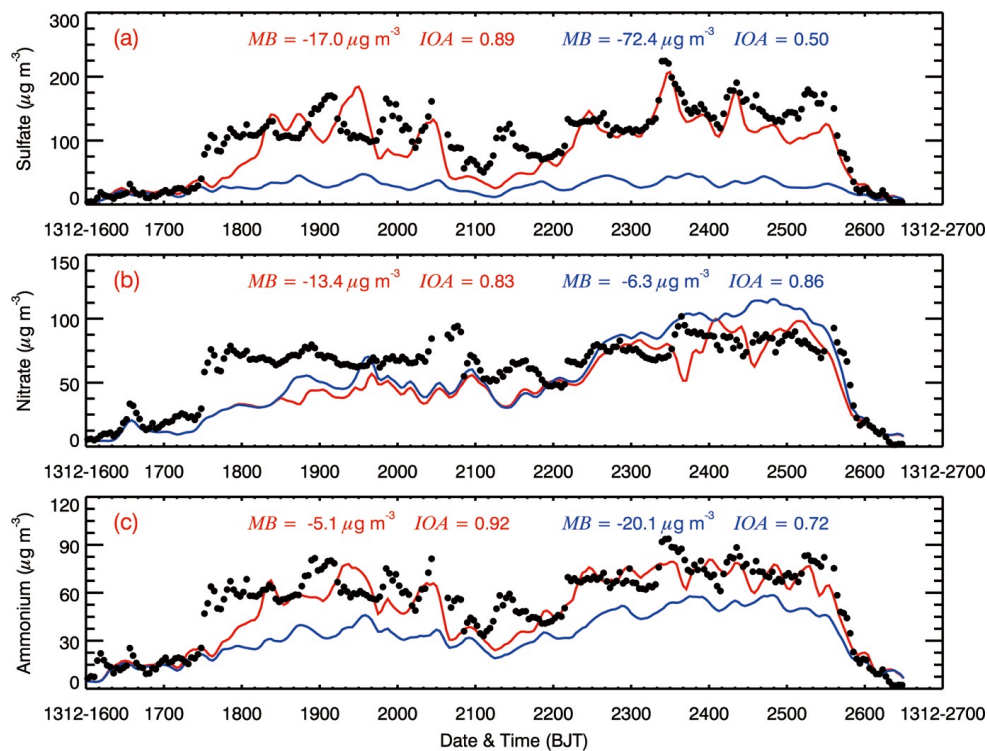
Figure 11 Comparison of measured and simulated diurnal profiles of inorganic aerosols of (a) sulfate, (b) nitrate, and (c) ammonium in Xi'an from 16 to 27 December 2013. The black dots represent the observations, and the solid red and blue lines denote the simulations in the E-case and B-case, respectively.
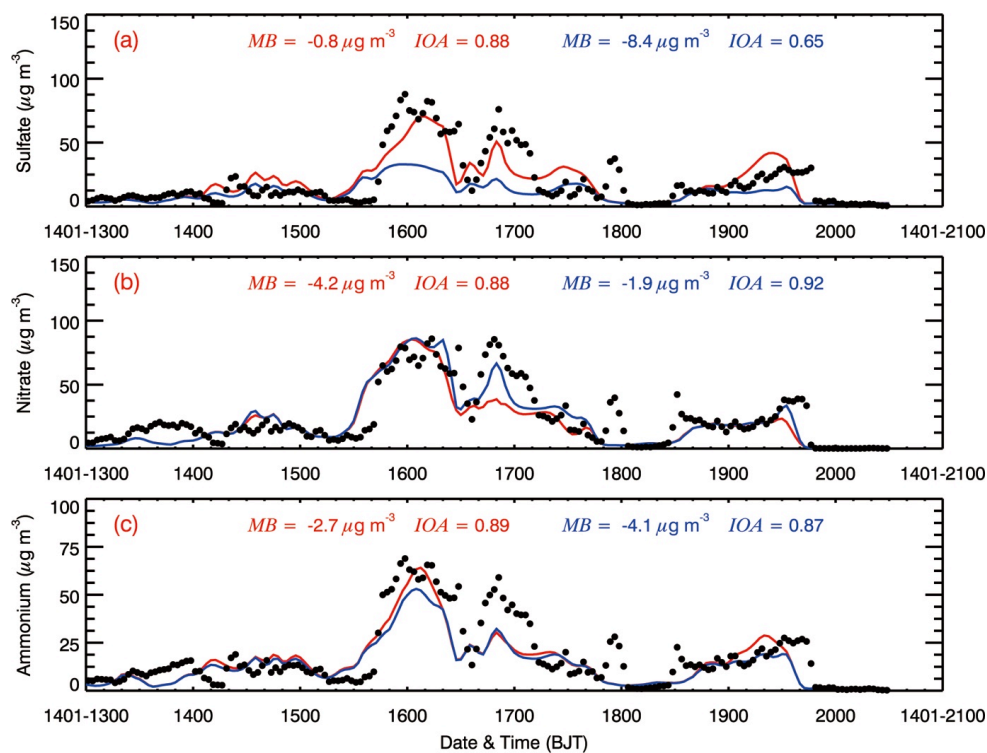
Atmospheric
Chemistry
and Physics
Discussions

765
766
767   Figure 12 Same as Figure 11, but in Beijing from 13 to 21 January 2014.
768
769
770
771
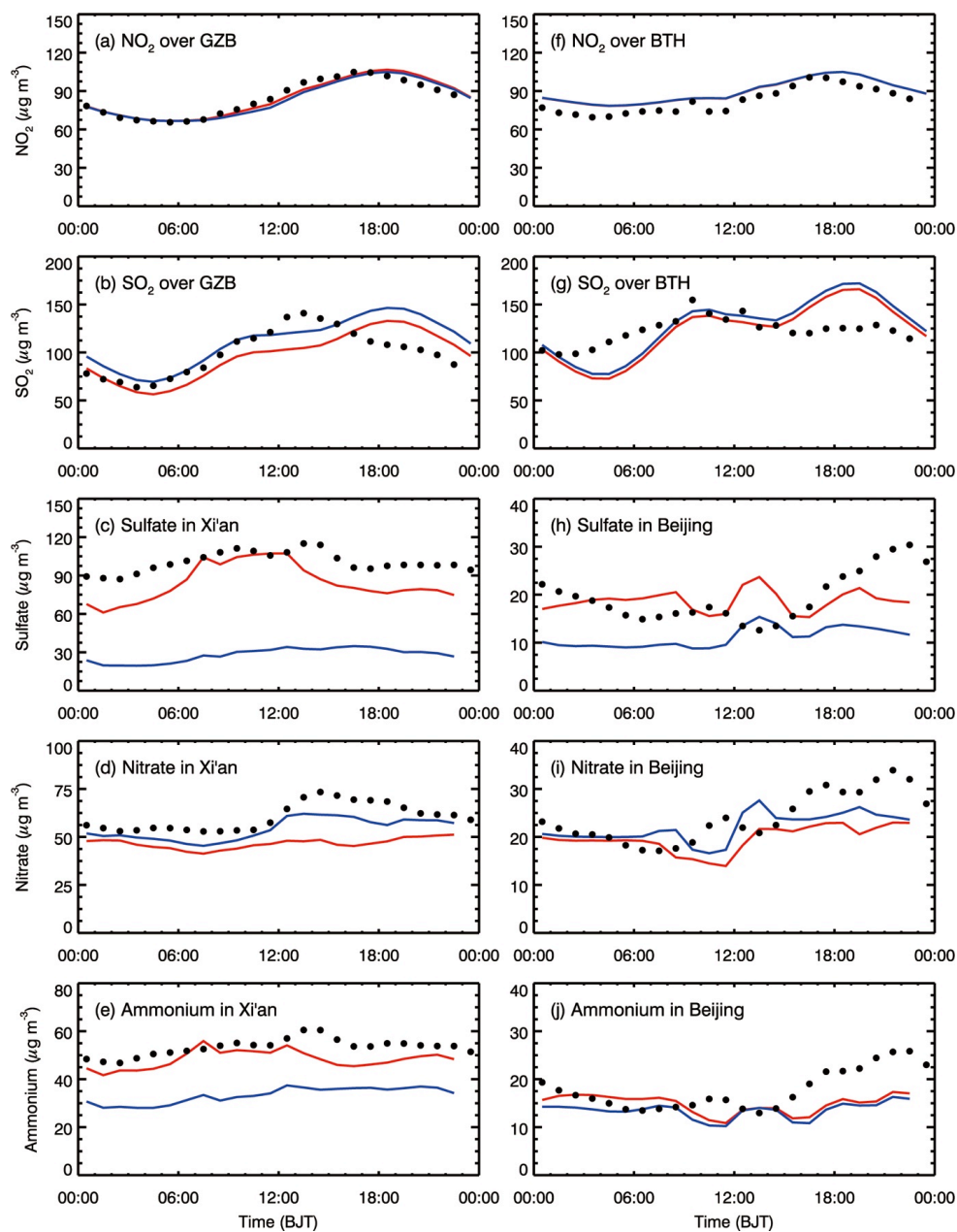
Figure 13 Observed and simulated diurnal cycles of mass concentrations of NO_2 and SO_2 averaged over GZB and BTH and the sulfate, nitrate, and ammonium aerosols in Xi'an and Beijing during the simulated episodes.

778
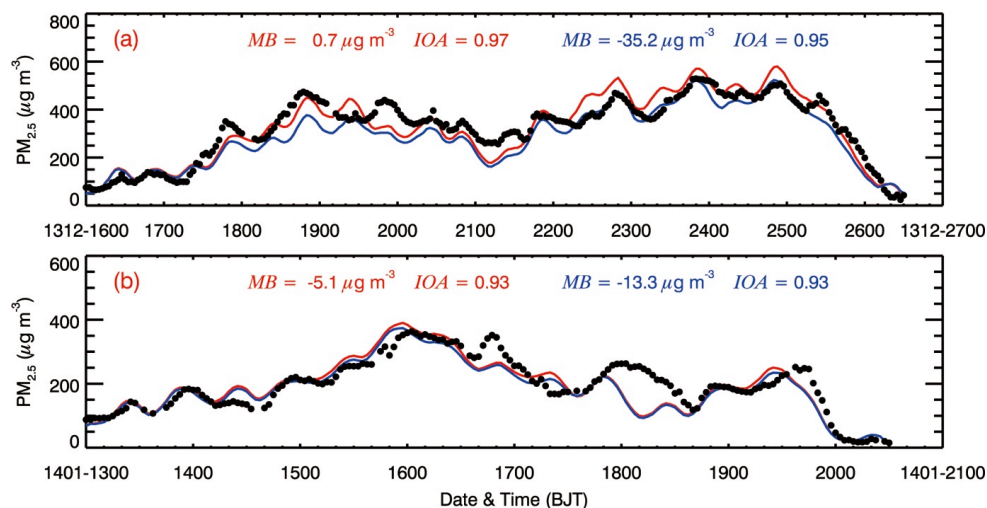
779
780
781 Figure 14 Comparison of measured and predicted diurnal profiles of near-surface hourly
782 PM$_{2.5}$ mass concentration averaged over all ambient monitoring stations (a) in GZB from 16
783 to 27 December 2013 and (b) in BTH from 13 to 21 January 2014. The black dots represent
784 the observations, and the solid red and blue lines are the simulations in the E-case and B-case,
785 respectively.
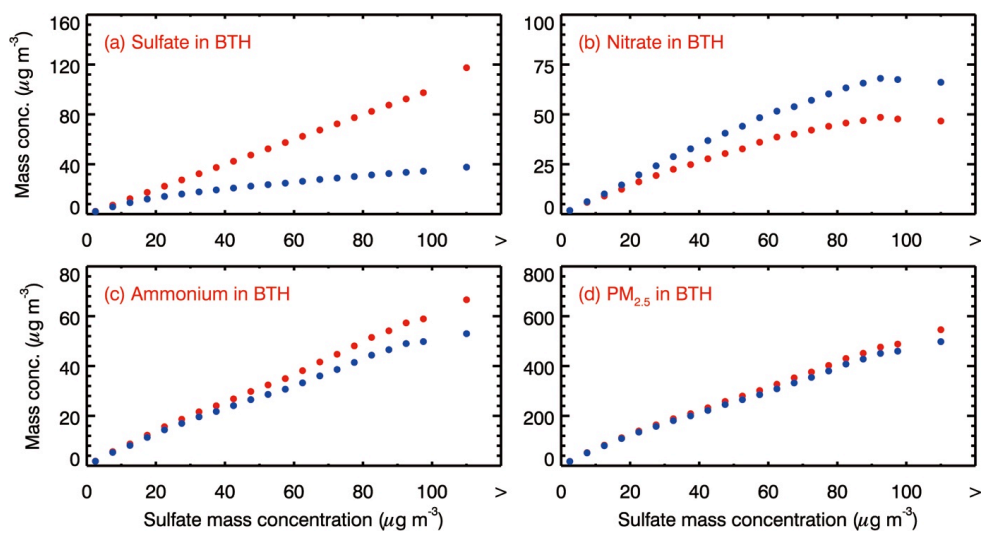786
787
788
789
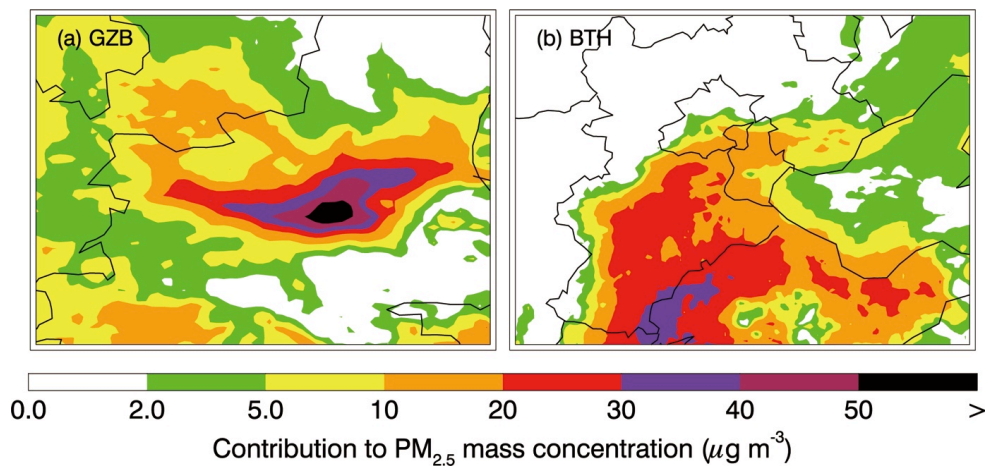
790
791
792 Figure 15 Distribution of the average near-surface $PM_{2.5}$ contribution due to the SO_2
793 heterogeneous reactions in GZB and BTH during the simulated episodes.
794
795
796
797
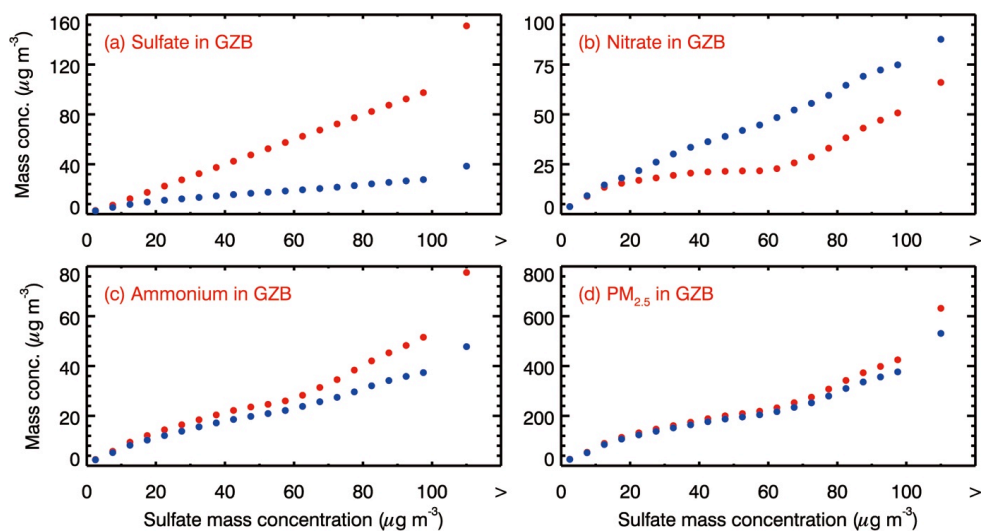
798
799
800 Figure 16 Average (a) sulfate, (b) nitrate, (c) ammonium, and (d) PM$_{2.5}$ mass concentrations
801 in GZB during the simulation period as a function of the sulfate mass concentration in the E-
802 case. The red and blue dots represent average mass concentrations in the E-case and B-case,
803 respectively.
804
805
806
807

Atmospheric
Chemistry
and Physics
Discussions

Open Access

EGU

808
809
810   Figure 17 Same as Figure 16, but in BTH from 13 to 21 January 2014.
811
812
813
814